2014 IEEE International Conference on Robotics & Automation (ICRA)
Hong Kong Convention and Exhibition Center
May 31 - June 7, 2014. Hong Kong, China

A Passive, Origami-Inspired, Continuously Variable Transmission

Samuel M. Felton[1], Dae-Young Lee[2], Kyu-Jin Cho[2], and Robert J. Wood[1]

***Abstract*— Transmissions play a vital role in machines by transforming the torque and speed of a motor into a desired output. They are often necessary for operating a motor at peak efficiency or power. The majority of variable transmissions are mechanically complex, large, and expensive, which limits scalability and is often cost prohibitive. As an alternative, we propose an origami-wheel design that is capable of varying its own transmission ratio between motor torque and ground reaction force, effectively creating a passive, continuously variable transmission. The wheel responds to an increase in torque by reducing its radius through the spring-like properties of the origami structure, increasing the force applied by the wheel to the ground. We demonstrate that the wheel is able to match the speed of a 55 mm fixed-radius wheel when unloaded, and can also tow loads as high as a 25 mm wheel without stalling. This design could be used to provide smaller, cheaper robots with an effective means to vary their output while maintaining motor efficiency.**

I. INTRODUCTION

The transmission is a necessary component of any machine; it transforms the power input from an actuator into the desired output by altering the speed and force. Traditional variable transmissions enable machines to operate efficiently at a wide range of speeds while allowing the actuator to operate close to peak power or efficiency, and for this reason can be found in many wheeled vehicles. The most common types of automobile transmissions are mechanically complex, and consist of a torque converter, a planetary gear train, and a hydraulic or manual controller [1]. Each of these components comprises many parts, making them large and expensive. These transmissions have a finite number of ratios, so they cannot operate at peak performance through a continuous range of speeds. In order to improve efficiency, automobile manufacturers have experimented with continuously variable transmissions (CVTs), which have an infinite number of transmission ratios, sometimes over an infinite range, using mechanical, hydraulic, or electrical controllers [1], [2], [3], [4], [5]. While sometimes more efficient, these systems are still mechanically complex, and have yet to replace traditional transmissions in many vehicles due to their larger size, higher cost, and/or lack of durability. In smaller or less expensive vehicles such as wheeled robots, these disadvantages make any kind of variable gearing prohibitive.

In order to reduce cost and complexity, we looked to develop a passive control system to vary the transmission ratio. Passive devices integrate mechanical intelligence into machine design in lieu of a distinct control system, and have been implemented at a variety of scales: a windshield wiper blade distributes an applied force across six points while being driven by a single rotary linkage, micro-air vehicles such as the Harvard Microrobotic Fly rely on passive wing rotation to achieve an optimal wing angle and maximize thrust [6], [7], and a transformable wheel can passively deploy or retract legs in order to adapt to smooth or rough terrain, using only external friction [8]. Passive mechanisms are also utilized in some cases because they behave more quickly and accurately. The differential mechanism in an automobile balances the torques applied to different wheels driven by the same motor, allowing them to rotate independently while simultaneously aiding in traction [6]. All of these devices rely on clever mechanical design to tighten the dynamic feedback loop.

In order to develop a new, passive CVT, we looked to harness the intrinsic mechanical properties of folded structures. Origami has inspired a variety of mechanisms that are less expensive and/or perform better than more traditional devices, including actuators [9] and springs [10]. Labor and material costs are reduced by harnessing two-dimensional materials and fabrication methods. These devices utilize fold geometry and material bending properties to extract significant function out of apparently simple designs. Entire robotic platforms have been constructed using these techniques [11],

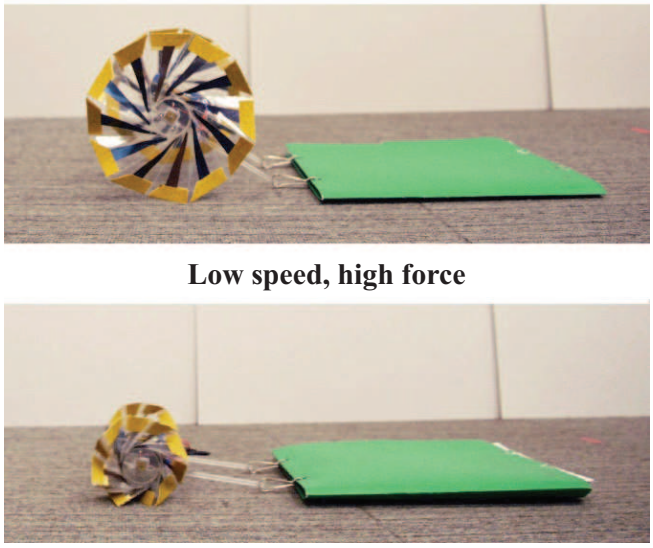

Fig. 1. The origami-inspired wheel passively adjusts the torque-force transmission ratio by altering its radius in response to a tangential load.

[1]Samuel Felton and Robert Wood are with the School of Engineering and Applied Sciences, Harvard University, Cambridge, MA 02138, USA, and the Wyss Institute for Biologically Inspired Engineering, Harvard University, Boston, MA 02115, USA. sam@seas.harvard.edu

[2]Dae-Young Lee and Kyu-Jin Cho are with the School of Mechanical and Aerospace Engineering, Seoul National University, Gwanak 1 Gwanak-ro, Gwanak-gu, Seoul 151-742, Korea winter2nf@gmail.com

[12], [13], [14], [15]. Particularly relevant to our goals, Lee et al. have demonstrated a suite of folding wheels actuated by shape memory alloy wire that can change shape in order to adapt to different environments [16], [17].

In this paper we demonstrate that origami-inspired wheels can be utilized passively to effect a continuously variable transmission (Fig. 1). This design responds to a changing tangential load by changing its radius, acting as a continuously variable transmission ratio between input torque and output force. We demonstrate the performance of these wheels by incorporating them into a machine towing varying loads, and compare it to fixed wheeled designs.

II. DESIGN

The origami wheel design consists of a polyester (PET) dodecagon with twelve fold lines extending to each vertex and tangent to an internal core of radius R_i (Fig. 2a). These lines are folded in opposite directions, resulting in faces whose normal vector is approximately orthogonal to the original plane of the paper and the wheel axis. This design is geometrically similar to the one used by Lee et al. [16].

When a torque is applied to the wheel and an opposing shear force applied to the wheel edge, an equivalent bending moment is applied to each radial face, causing that face to wrap around the core. A larger torque results in more bending, which decreases the effective radius of the wheel. The decreased radius, in turn, results in an increased transmission ratio between wheel torque and corresponding tangential force. The fold pattern maintains continuity of the outer edge of the wheel and ensures that all of the faces fold together, so that the wheel maintains a more circular shape than a set of unconnected, radial spring plates would.

Spring steel plates are attached to each face in order to increase stiffness. These plates are shaped to form a triangle whose width is 1/3 of the PET face width, and is truncated to 70 mm length in order to prevent interference at the core of the wheel (Fig. 2b). Acrylic plates are attached to the core of the wheel on both sides to maintain rigidity and couple with a motor shaft (Fig. 2c). These plates have a slightly smaller diameter than the core of the origami pattern in order to avoid interference with the fold pattern.

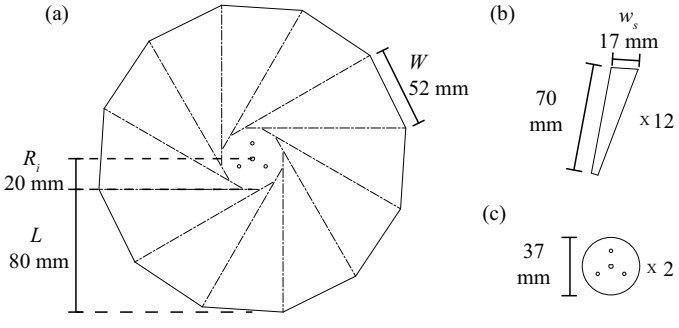

Fig. 2. A drawing of the components of the origami wheel. (a) A dodecagon is cut out of PET, with 12 perforated fold lines. R_i is the core radius, L is the length of the bending faces, and W is the width of each face at the outer edge. (b) 12 steel plates are cut and adhered to the 12 faces of the wheel. w_s is the width of the steel plate at the outer edge of the wheel.(c) The core of the wheel is sandwiched between two acrylic plates to provide rigidity and enable coupling to the motor shaft.

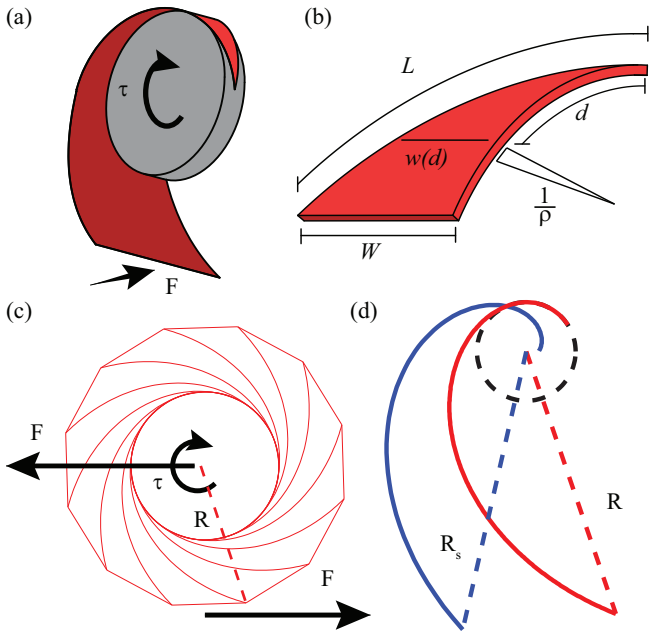

Fig. 3. (a) Each face (red) experiences a bending moment τ and a tangential reaction force F. The moment causes the beam to bend and wrap around the core (gray). (b) Each face of the wheel is modeled as a beam with a variable width w dependent on the distance d from its interior end. The total length of the face is L, and the maximum width is W. This face exhibits a variable curvature ρ when under load. (c) Free body diagram of the wheel undergoing a drag force and reaction ground force, as well as a moment. The bending moment is spread between all faces, so that each face follows the same curve, resulting in an effective radius R of the wheel. (d) A logarithmic spiral (blue) and the path of a single face of the origami wheel (red). The face is constrained to a maximum curvature by the core of the wheel, indicated by the dotted line. However, the maximum radii of both curves (R_s and R) are approximately equal.

III. MODEL

The model of the origami wheel assumes that the primary mode of deformation contributing to wheel stiffness is the bending of the faces tangentially to the core (Fig. 3a). Each face is modeled as a beam whose width w increases linearly as a function of the distance d along the length of the face (Fig. 3b). Each plate's local bending stiffness k_f can be calculated by treating the face as a composite of the steel and PET layers, and the total stiffness k of the wheel is assumed to be due to the 12 faces of the wheel bending in parallel so that $k = 12k_f$ (Fig. 3c). Because k is dependent on w

$$k(d) = k'w(d) = k'W\frac{d}{L} \tag{1}$$

where k' is the stiffness per unit width, W is the maximum width of the face, and L is the total length of the face. When a bending moment is applied, the face exhibits a curvature ρ, calculated as

$$\rho = \frac{\tau}{k} = \frac{\tau L}{k'Wd} \tag{2}$$

that is inversely proportional to d. Therefore, the curve of the beam is similar to that of a logarithmic spiral [18], which can be expressed in cylindrical coordinates as

$$r = ae^{b\theta} \tag{3}$$

where a and b are coefficients defining the spiral, and whose arc length s is inversely proportional to its curvature ρ_s. In cylindrical coordinates, the radial coordinate of this spiral can be expressed as a function of arc length

$$r(s) = \frac{sb}{\sqrt{1+b^2}} \tag{4}$$

The curvature of a logarithmic spiral is given as

$$\rho_s = \frac{1}{sb} \tag{5}$$

and we assume that $\rho = \rho_s$ and $s = d$, so that eqs. 2 and 5 can be combined to solve for b.

$$b = \frac{k'W}{\tau L} \tag{6}$$

The maximum radius R_s of the spiral with a total arc length $s = L$ is defined as $R_s = r(L)$, and we assume that the radius of the wheel $R \approx R_s$ (Fig. 3d). This approximation was verified to be accurate to within 2% by numerical analysis, given the parameter values used in this paper and over the range of torques the motors were capable of producing.

τ is equal to the ground reaction force F multiplied by R, which can be expressed as a function of b.

$$\tau = FR = \frac{FbL}{\sqrt{1+b^2}} \tag{7}$$

Eqs. 6 and 7 can be combined to solve for the torque explicitly:

$$\tau = \sqrt{\frac{-\left(\frac{k'W}{L}\right)^2 + \sqrt{\left(\frac{k'W}{L}\right)^4 + 4\left(k'WF\right)^2}}{2}} \tag{8}$$

From here, the radius, radial velocity, and vehicle speed can be calculated. The transmission ratio TR between ground force and torque is simply the inverse of the radius.

$$TR = \sqrt{\frac{2F^2}{-\left(\frac{k'W}{L}\right)^2 + \sqrt{\left(\frac{k'W}{L}\right)^4 + 4\left(k'WF\right)^2}}} \tag{9}$$

When applying this model to predicting vehicle speed, we assume that the drag load is equal to $2F$, the motors are under a constant voltage, and that there is an inverse linear relationship between motor torque and angular velocity, so that

$$\omega = \omega_{max}\left(1 - \frac{\tau}{\tau_{max}}\right) \tag{10}$$

The values used for these calculations are shown in table I, and the resulting models are included in figures 5 and 6.

TABLE I

VALUES USED TO MODEL WHEEL STIFFNESS AND VEHICLE SPEED

Face length	L	80 mm
Core radius	R_i	20 mm
PET Young's modulus	E_p	3 GPa
PET thickness	t_p	125 μm
Maximum PET width	W	52 mm
Steel Young's modulus	E_s	207 GPa
Steel thickness	t_s	50 μm
Maximum steel width	w_s	17 mm
Specific stiffness	k'	45.2 mN-m
Motor stall torque	τ_{max}	50 mN-m
Motor free speed	ω_{max}	12 rad/s

IV. EXPERIMENTAL SETUP

The effective stiffness of the wheel was measured by applying a point load to the edge of the wheel, in the form of a hook and mass (Fig. 4). Three separate measurements were taken at each load by applying the mass to three different points along the wheel. The effective radius was measured from the center of the wheel to the edge closest to the applied mass. A picture was taken for each measurement, and the distance was measured using ImageJ analysis software.

In order to measure the effect of wheel design on vehicle speed, three different sets of wheels were produced: The origami-inspired design, as well as large and small fixed-radius wheels for experimental controls. The large wheels were 6.4 mm wide and had a radius of 55 mm, and were used as a reference for the maximum speed of the origami wheel. The small wheels, 12.7 mm wide and 25 mm in radius, acted as a reference for the maximum load. These widths were chosen to match the mass of the control wheels to that of the origami wheels while also preventing slippage. Sandpaper was applied to the edge of all wheels in order to increase friction and prevent slippage between the wheels and the ground. A chassis was used for testing that consisted of an acrylic frame, two electric motors (100-1 Micro Metal Gearmotor, Pololu) 170 mm apart, a controller (Uno R3, Arduino), and motor shield (Motor/Stepper/Servo Shield for Arduino, Adafruit) to drive the motors. The controller and motor shield were powered by separate batteries (2S 120mAh

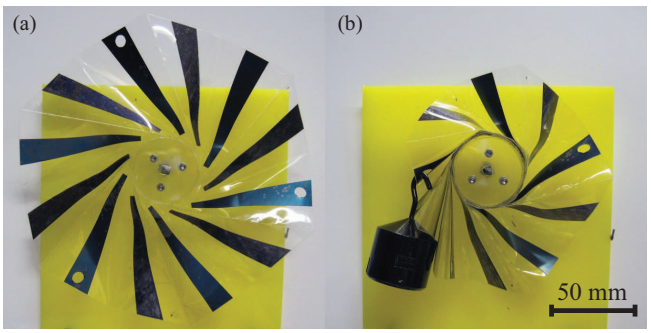

Fig. 4. The effective stiffness of the origami wheel was measured by applying a point load to the edge. (a) The unloaded wheel. (b) The wheel loaded with 200 g.

20C LiPo, E-flite) with a measured output ranging from 8.0 to 8.3 V. In order to simulate a varying drag load, a folder was attached to the chassis at two points 130 mm behind the motors, and loaded with paper to adjust friction between the folder and the carpet (Fig. 1).

All speed experiments were run on carpet over a distance of two meters, and speed was measured via video recording with a digital camera (Powershot A1100 IS, Canon). Motors were run at a constant voltage. The drag load was varied by increments of 0.4 N, from 0.1 N to 2.9 N. Five samples were run at each load for each wheel configuration.

V. FABRICATION

The Origami wheel consists primarily of 125 μm thick PET. Fold lines were perforated in the PET, and folded by hand. 50 μm spring steel was cut with a table-mounted paper cutter and attached to the PET using acrylic tape (Scotch 926 High Performance, 3M). 18.5 mm radius plates were cut from 3.2 mm acrylic and attached to the core via screws in order to maintain rigidity of the core and allow motor attachment via press fitting. The chassis was cut from 3.2 mm acrylic, and the fixed-radius wheels were cut from 6.4 mm acrylic. Unless otherwise noted, all cuts were made with a commercial CO2 laser machining system (VLS 2.3, Universal Laser Systems).

VI. RESULTS

The measured and modeled stiffnesses of the origami wheel are shown in figure 5 by plotting the effective radius as a function of tangential load. The actual stiffness was higher than expected. This may be due to the additional sources of energy storage in the wheel geometry. For instance, the faces undergo twisting as well as bending as they wrap around the core, which would make the wheel effectively stiffer. In addition, the model treats our faces as an ideal composite

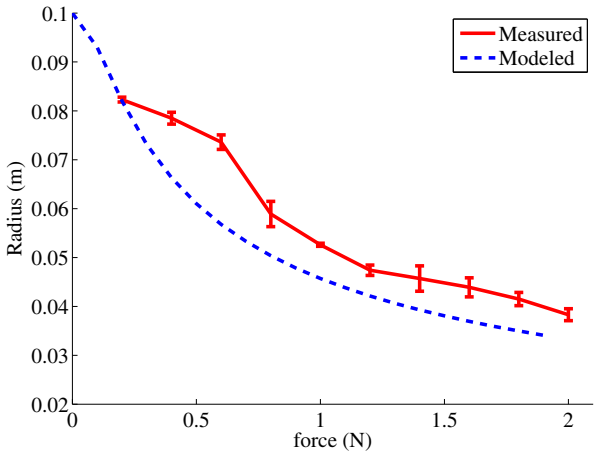

Fig. 5. The measured and modeled radii of the origami wheel as a function of a tangential force on the wheel's edge. The radius represents the inverse of the transmission ratio from the motor torque to the ground force. Each load was applied to the wheel separately at three different points along its edge for three independent measurements. Error bars indicate the standard deviation of the measured radius.

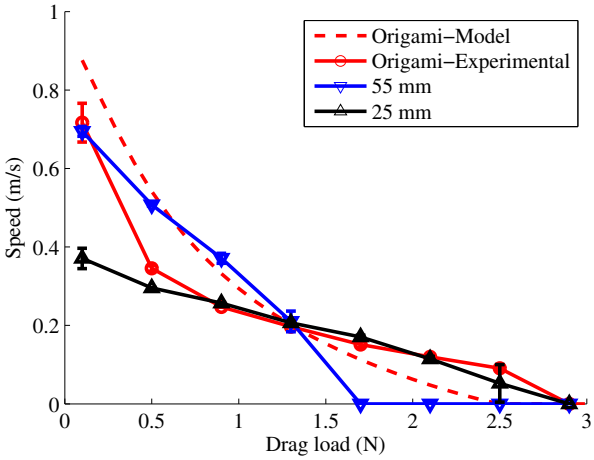

Fig. 6. The speed of the test machine utilizing each wheel as a function of drag load, as well as the modeled speed expected from the origami wheel. Five trials were measured for each load and wheel design. Error bars indicate the standard deviation of the measured speed. Some error bars are too small to be visible.

for the purposes of calculating area moment, but in fact, the adhesive between the two layers may affect this moment. Finally, the deformed wheel did not maintain a perfectly circular edge, but instead deformed more near the load point, so the assumption of equal displacement of all 12 faces may result in some inaccuracy.

The measured speed of the test machine utilizing each wheel is shown as a function of drag load in figure 6. The fixed-radius wheels performed as expected, demonstrating an approximately linear relation between load and speed. One notable exception to this trend is that the smaller wheels began to slip at a load of 2.5 N, resulting in a smaller maximum load and greater standard deviation than was expected.

The origami wheel demonstrated a speed equivalent to the larger fixed-radius wheel at the minimum load of 0.1 N. At higher loads, it exhibited speeds more similar to those of the smaller wheel (see Supp. Video). It stalled at a load of 2.9 N, the same as the smaller wheel. It also exhibited some amount of slipping at loads of 0.5 N and higher, which contributed to the origami wheels' underperformance at loads between 0.5 N and 1.3 N compared to the 55 mm wheel. Overall, the origami wheel performed as well as the faster of the two fixed-radius wheels at every load except 0.5 N and 0.9 N, and never performed worse than both.

The model overestimated the speed at lower loads, and underestimated it at higher loads. The difference between the model and experiments at low loads can be explained by slippage, which our model did not take into account. Greater slippage at higher speed is likely because the contact area between the wheel and the ground is smaller. When the wheel is expanded, the effective width of the wheel is not much greater than the thickness of the PET; while the wheel is contracted, the width is equal to the maximum face width (Fig. 7). At higher loads, the difference between the

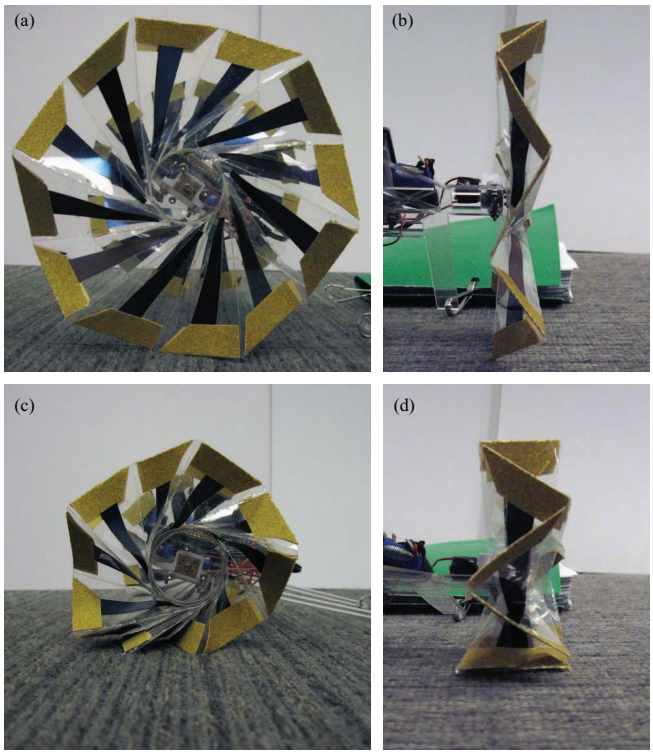

Fig. 7. As the radius of the wheel decreases, the effective width and traction of the wheel increase. Pictured here are the side (a) and front (b) views of the wheel in its relaxed state and under no load, as well as the side (c) and front (d) views of the wheel at its minimum radius when the motors are exerting their stall torque.

model and the data may be due to a more complex force-displacement profile than the model accounted for, or gravity may be causing additional deformation, resulting in a smaller wheel and a more advantageous force-torque ratio.

For further comparison, we installed the origami wheels backwards and then measured the machine's unloaded speed. When the wheels are run in reverse, the tangential force pushes the wheels open so that they hold a maximum radius. When run this way, the machine moved at a speed of 0.8 ± 0.02 m/s. If this wheel is in a configuration where it can be utilized in reverse, this technique can be used to achieve an even greater range of speeds.

VII. DISCUSSION

The origami wheel demonstrated speeds equivalent to the larger fixed-radius wheel when unloaded, but was able to output up to 90% more force without stalling. These results indicate that this wheel is better-suited to handling a wide variety loads than fixed-radius wheels, and can passively respond to changes in load to match motor input to vehicle output. The integration of the transmission and the wheel makes installation and repair faster and less expensive. The wheel could be modified for different ranges of torques by altering the wheel stiffness. In addition, these wheels are inexpensive to produce; material costs for the origami wheel total $1.50, compared to $2.10 for the larger fixed-radius wheel.

This design can be used to improve wheeled robots in a variety of applications. It's simplicity eliminates the multiple components found in other transmissions while its ease of installation enables replacement at the user level . These features are ideal for unmanned ground vehicles that are used for reconnaissance and ordinance disposal in environments where logistic support is limited and performance is critical [19]. It can also be used with planetary exploration rovers when transportation volume is limited [20], [21]. The wheel can be compressed into its smallest configuration during interstellar flight, and the purely mechanical transmission would reduce the weight and volume of the robot.

In addition to wheeled vehicles, this design has the potential for placement in other devices. By applying appropriate constraints, such as bracketing the wheel with plates on both sides, this design could be used with pulleys or belts to create a variable transmission in other underactuated devices [22]. A tire that could adjust size with the wheel would improve road friction and allow for further customization to specific needs. A bistable component may also allow this wheel to be used as a discretely variable transmission as well.

Improvements could be made to performance by altering the force-displacement curve of the spring. If the wheel were stiffer at moderate loads, the origami wheel might perform as well as the large fixed-radius wheel up to the inflection point when the smaller wheel performs better. This would have the added benefit of widening the power profile, allowing the motor to operate at peak efficiency over a larger range of loads. Changes in materials and folding techniques may also reduce slippage and maintain a more even deformation across the circumference; The uneven displacement of the faces means that each spring is absorbing and then releasing energy, resulting in an overall loss. Finally, it is theoretically possible to improve the range of transmission ratios, but this involves increasing the ratio of the maximum radius to the core radius, which is limited by the folding mechanics of the substrate and the folding technique. Improvements to either of these would expand the operational loading range of the wheel.

ACKNOWLEDGMENT

The authors gratefully acknowledge support from the National Science Foundation (award number CCF-1138967) and the National Defense Science and Engineering Graduate Fellowship program. Any opinions, findings, and conclusions or recommendations expressed in this material are those of the authors and do not necessarily reflect those of the National Science Foundation.

REFERENCES

[1] P. G. Gott, *Changing Gears: The Development of the Automotive Transmission*. Warrendale, PA: Society of Automotive Engineers, Inc., 1991.

[2] N. Srivastava and I. Haque, "A review on belt and chain continuously variable transmissions (CVT): Dynamics and control," *Mechanism and machine theory*, vol. 44, no. 1, pp. 19–41, 2009.

[3] J. M. Miller, "Hybrid electric vehicle propulsion system architectures of the e-CVT type," *Power Electronics, IEEE Transactions on*, vol. 21, no. 3, pp. 756–767, 2006.

[4] J. M. Miller and M. Everett, "An assessment of ultra-capacitors as the power cache in Toyota THS-II, GM-Allision AHS-2 and Ford FHS hybrid propulsion systems," in *Applied Power Electronics Conference and Exposition, 2005. APEC 2005. Twentieth Annual IEEE*, vol. 1, pp. 481–490.

[5] P. Kanphet, P. Jirawattana, and B. Direcksataporn, "Optimal operation and control of a hydrostatic CVT powertrain," *SAE transactions*, vol. 114, no. 6, pp. 1838–1845, 2005.

[6] P. S. Sreetharan and R. J. Wood, "Passive aerodynamic drag balancing in a flapping-wing robotic insect," *Journal of Mechanical Design*, vol. 132, p. 051006, 2010.

[7] P. S. Sreetharan and R. J. Wood, "Passive torque regulation in an underactuated flapping wing robotic insect," *Autonomous robots*, vol. 31, no. 2-3, pp. 225–234, 2011.

[8] Y.-S. Kim, G.-P. Jung, H. Kim, K.-J. Cho, and C.-N. Chu, "Wheel transformer: A miniaturized terrain adaptive robot with passively transformed wheels," in *IEEE Int. Conf. on Robotics and Automation (ICRA)*. IEEE, 2013, pp. 5605–5610.

[9] H. Okuzaki, T. Saido, H. Suzuki, Y. Hara, and H. Yan, "A biomorphic origami actuator fabricated by folding a conducting paper," in *Journal of Physics: Conference Series*, vol. 127. IOP Publishing, 2008, p. 012001.

[10] C. C. Min and H. Suzuki, "Geometrical properties of paper spring," *Manufacturing Systems and Technologies for the New Frontier*, pp. 159–162, 2008.

[11] J. P. Whitney, P. S. Sreetharan, K. Y. Ma, and R. J. Wood, "Pop-up book MEMS," *Journal of Micromechanics and Microengineering*, vol. 21, no. 11, p. 115021, 2011.

[12] P. S. Sreetharan, J. P. Whitney, M. D. Strauss, and R. J. Wood, "Monolithic fabrication of millimeter-scale machines," *Journal of Micromechanics and Microengineering*, vol. 22, no. 5, p. 055027, 2012.

[13] C. D. Onal, R. J. Wood, and D. Rus, "Towards printable robotics: Origami-inspired planar fabrication of three-dimensional mechanisms," in *IEEE Int. Conf. on Robotics and Automation (ICRA)*. IEEE, 2011, pp. 4608–4613.

[14] C. D. Onal, R. J. Wood, and D. Rus, "An origami-inspired approach to worm robots," *IEEE/ASME Transactions on Mechatronics*, vol. 18, no. 2, pp. 430–438, 2012.

[15] S. M. Felton, M. T. Tolley, C. D. Onal, D. Rus, and R. J. Wood, "Robot self-assembly by folding: A printed inchworm robot," in *IEEE Int. Conf. on Robotics and Automation (ICRA)*. IEEE, 2013, pp. 277–282.

[16] D.-Y. Lee, G.-P. Jung, M.-K. Sin, S.-H. Ahn, and K.-J. Cho, "Deformable wheel robot based on origami structure," in *IEEE Int. Conf. on Robotics and Automation (ICRA)*. IEEE, 2013, pp. 5592–5597.

[17] D.-Y. Lee, J.-S. Kim, S.-R. Kim, J.-S. Koh, and K.-J. Cho, "The deformable wheel robot using magic-ball origami structure," in *Proc. of the ASME 2013 Int. Design Engineering Technical Conf. & Computers and Information in Engineering Conf. (IDETC/CIE)*. ASME, 2013.

[18] E. W. Weisstein. Logarithmic spiral. From MathWorld–A Wolfram Web Resource. Visited 11August2013. [Online]. Available: http://mathworld.wolfram.com/LogarithmicSpiral.html

[19] M. R. Blackburn, R. T. Laird, and H. R. Everett, "Unmanned ground vehicle (UGV) lessons learned," DTIC Document, Tech. Rep., 2001.

[20] S. Hirose, "Variable constraint mechanism and its application for design of mobile robots," *The International Journal of Robotics Research*, vol. 19, no. 11, pp. 1126–1138, 2000.

[21] T. Aoki, Y. Murayama, and S. Hirose, "Mechanical design of three-wheeled lunar rover; 'Tri-Star IV'," in *Robotics and Automation (ICRA), 2011 IEEE International Conference on*. IEEE, 2011, pp. 2198–2203.

[22] S. A. Spanjer, R. Balasubramanian, A. M. Dollar, and J. L. Herder, "Underactuated gripper that is able to convert from precision to power grasp by a variable transmission ratio," in *Advances in Reconfigurable Mechanisms and Robots I*. Springer, 2012, pp. 669–679.